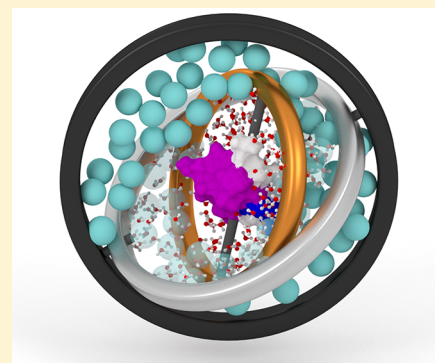


Multiscale Simulation of Protein Hydration Using the SWINGER Dynamical Clustering Algorithm

Julija Zavadlav,[†] Siewert J. Marrink,[‡] and Matej Praprotnik^{*,§,¶,Ⓜ}[†]Computational Science & Engineering Laboratory, ETH Zurich, Clausiusstrasse 33, CH-8092 Zurich, Switzerland[‡]Groningen Biomolecular Sciences and Biotechnology Institute and Zernike Institute for Advanced Materials, University of Groningen, Nijenborgh 7, 9747 AG Groningen, The Netherlands[¶]Laboratory for Molecular Modeling, National Institute of Chemistry, Hajdrihova 19, SI-1001 Ljubljana, Slovenia[§]Department of Physics, Faculty of Mathematics and Physics, University of Ljubljana, Jadranska 19, SI-1000 Ljubljana, Slovenia

ABSTRACT: To perform computationally efficient concurrent multiscale simulations of biological macromolecules in solution, where the all-atom (AT) models are coupled to supramolecular coarse-grained (SCG) solvent models, previous studies resorted to modified AT water models, such as the bundled-simple point charge (SPC) models, that use semiharmonic springs to restrict the relative movement of water molecules within a cluster. Those models can have a significant impact on the simulated biomolecules and can lead, for example, to a partial unfolding of a protein. In this work, we employ the recently developed alternative approach with a dynamical clustering algorithm, SWINGER, which enables a direct coupling of original unmodified AT and SCG water models. We perform an adaptive resolution molecular dynamics simulation of a Trp-Cage miniprotein in multiscale water, where the standard SPC water model is interfaced with the widely used MARTINI SCG model, and demonstrate that, compared to the corresponding full-blown AT simulations, the structural and dynamic properties of the solvated protein and surrounding solvent are well reproduced by our approach.



1. INTRODUCTION

Dual-resolution molecular dynamics (MD) schemes,^{1–3} where one part of the system is modeled at a high resolution atomistic (AT) detail and the other part at a low coarse-grained (CG) resolution level, continue to be an active research area due to their possibility to provide the same level of accuracy as the AT simulations at a fraction of their computational cost. In the context of biomolecular simulations, it is typically the solvent region that is treated on a simplified level as it is both computationally the most cumbersome part and, furthermore, not a region of a particular interest.

Based on whether the solvent molecules' resolution is kept fixed throughout the course of the simulation or is allowed to change as the molecules move between predefined spatial resolution regions, the dual-resolution methods can be split into fixed resolution and concurrent schemes, respectively. The fixed resolution methods face major challenges essentially because the CG solvent models are, in general, not compatible with the established AT force fields. One way of solving this problem is to parametrize an AT force field for a particular CG solvent, such as the PACE force field for proteins in MARTINI solution.^{4,5} The other way is to use the existing force fields and define the AT–CG interactions. The latter can be specified and, if needed, reparametrized via mixing rules,^{6–9} parametrization of interactions,^{10–13} force matching,^{14,15} or indirect definition using the virtual sites.^{16–18} Yet another way is to

consider the distal solvent in an implicit manner, that is, with the hybrid discrete/continuum solvent approaches.^{19–24}

In terms of reproducing the all-atom simulation results, many of these methods have been quite successful. Nevertheless, in situations where hydrogen-bonding interactions between water and the biomolecule play a significant role, the treatment of water on a CG level is still oversimplified.²⁵ Moreover, direct coupling with CG water can also lead to serious side effects, such as complete unfolding of a protein.¹⁸ For these instances, a layer of AT water around biomolecules is recommended.^{18,26} Unfortunately, such a partitioning of the solvent requires restrictions for holding the AT water in the vicinity of the biomolecules, while keeping the CG water far away.^{18,26–28} As these restrictions are nonphysical, they produce artifacts such as too high density of the AT solvent²⁸ and the overstabilization of the biomolecule's native structure.¹⁸

These restraints can be avoided with concurrent multiscale approaches^{29–33} such as the Adaptive Resolution Scheme (AdResS)^{2,34–36} or its extensions, for example, Grand-Canonical-like version (GC-AdResS),^{37–40} Hamiltonian (H-AdResS),^{41–43} or Open Boundary Molecular Dynamics,^{44–47} but at the cost of an extra intermediate region that ensures a smooth transition between resolution levels. AdResS or AdResS-like methods can be also used for equilibration of

Received: November 9, 2017

Published: February 13, 2018

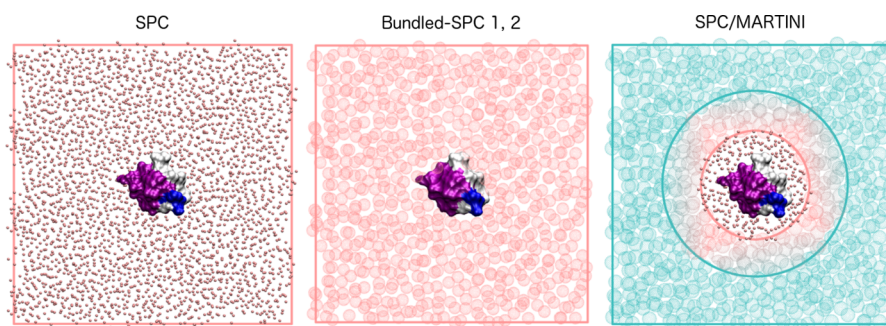


Figure 1. Schematic representation of the simulated systems. The left and central panels present the protein embedded in the fully atomistic solvent modeled with SPC⁶³ (red dots) and bundled-SPC⁵⁸ (red spheres) water model, respectively. The right panel depicts the multiscale solvation where high resolution SPC model is used for the water molecules in a spherical layer surrounding the protein, which is embedded in a bulk solvent modeled by the low resolution MARTINI model⁶⁴ (blue spheres).

molecular or complex liquids by reverse mapping from the CG to AT descriptions.^{44,48,49} So far, the AdResS has been applied to several biomolecular systems, such as proteins^{50–53} and nucleic acids^{54–57} in multiscale solutions, where the AT solvent models were coupled to either molecular CG models (1 molecule mapped to a CG bead) or supramolecular coarse-grained (SCG) models (several molecules mapped to a SCG bead). The latter offer greater speed increase and can accommodate coupling to the well-established MARTINI force field. On the other hand, this coupling is not straightforward because the scheme uses a center-of-mass (COM) based correspondence between low and high resolution representations, which cannot be used as long as the molecules diffuse far away from each other. Thus, it requires the use of either artificial AT bundled water models^{50,58–61} to accommodate a constant mapping or the recently developed dynamical mapping algorithm SWINGER⁶² that redistributes the molecules into CG beads on-the-fly.

In the present article, we report an AdResS MD simulation of an atomistic protein in a multiscale simple point charge (SPC)/MARTINI solution. From the surface of the protein to the simulation box edges, the representation of water is initially atomistic (standard SPC model) and then clustered with SWINGER into groups (each containing 4 water molecules), and finally each cluster is modeled as a MARTINI CG bead. We consider a 20-residue protein Trp-Cage to be a good test system since it is a fast folding and well-studied protein. Several properties of the protein and the solvent are investigated. We use the full-blown all-atom simulations as a reference to our multiscale simulation. Additionally, to highlight the artifacts that the bundled water models produce, we also perform all-atom simulations employing the two currently existing bundled-SPC water models.

2. METHODS AND COMPUTATIONAL DETAILS

We perform MD simulations of the Trp-Cage (pdb entry 1L2Y) protein in various water model solvents at ambient conditions. Figure 1 shows schematic depictions of the performed simulations. The protein is modeled on the AT scale using the GROMOS 54a7 force field.⁶⁵ The water is modeled either with fully atomistic (SPC⁶³ or bundled-SPC⁵⁸ model) or mixed AT/SCG resolution. For the bundled-SPC solvation, we test two models; that is, models 1 and 2 defined in ref 58. In the multiscale simulation, the solvent's level of representation depends on the distance to the protein's COM. We use the SPC⁶³ and MARTINI^{64,66} water models for the AT

($R < R_{AT}$) and SCG ($R > R_{SCG}$) domains, respectively. Thus, the boundaries between the resolution domains are spherical. We set the size of the atomistic sphere radius to $R_{AT} = 2.0$ nm to ensure a sufficient layer of all-atom solvent. Note that the center of the AT region sphere moves along with the protein's COM. The MARTINI model treats 4 water molecules as a single chargeless site. Thus, the mapping is 4-to-1. To facilitate such coupling, we employ the SWINGER algorithm that dynamically makes, breaks, and remakes clusters. The detailed description of the algorithm is reported in ref 62. Here, we briefly recapitulate its major algorithmic steps. The algorithm breaks the clusters that have moved to the AT region and makes or remakes clusters in a predefined “cluster formation” region C (see Figure 2). In this work, the region C is 0.2 nm thick, bordering the edge of the AT domain ($R_B < R < R_{AT}$; $R_B = R_{AT} - 0.2$ nm). The algorithm's output is an optimal grouping of water molecules into clusters, where each cluster

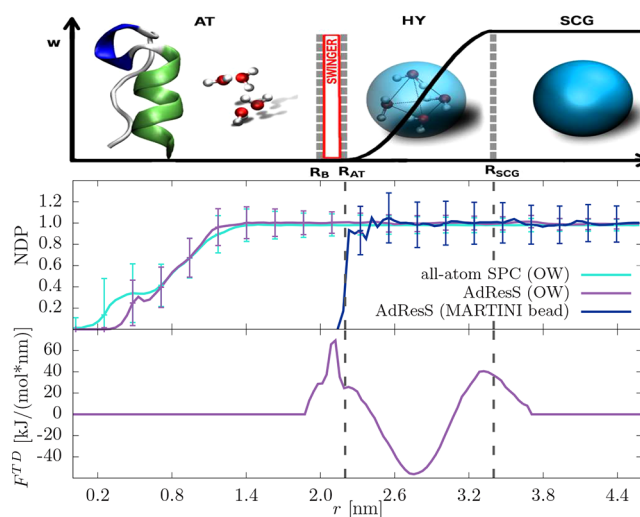


Figure 2. (top) Schematic representation of the multiscale simulation setup showcasing the employed models. In this work, we use the “reverse” implementation of AdResS, where $w = 0$ and 1 in the AT and SCG domains, respectively. Boundaries between the regions are marked with dotted gray lines, whereas the region C, where the clusters are formed, is framed with red lines. (middle) NDP (with standard deviation denoted by the error bars) around the COM of the protein for water oxygen atoms and MARTINI SCG beads. The multiscale results are compared to all-atom SPC solvations. (bottom) TD force that acts on bundles' COM mainly in the HY region.

contains exactly 4 water molecules. The optimal grouping is achieved with the initial grouping in an orderly fashion and the simulated annealing Monte Carlo-based refinement. Computational costs of the SWINGER algorithm depend on the size of the clustering region. In particular, the algorithm's complexity scales linearly with the number of water molecules examined for reclustering since the energy of the simulated annealing MC involves only intracluster contributions. When the algorithm is executed, the measured computational time of the MD time step is increased by approximately 5%. However, we do not initiate the SWINGER scheme at every time step but at every Verlet list update because the typical time scale of waters' tetrahedral cluster is on the order of a picosecond. Thus, the overall increase in the computational load due to SWINGER itself is negligible.⁶² When the clusters are formed a half-harmonic spring interaction is added between the oxygen atoms within a cluster. This bundled interaction is introduced gradually to avoid any large forces due to bundling and accommodate an easier reclustering as reported in ref 67.

The high and low resolution regimes are coupled via a force interpolation scheme,⁶⁷ where the total force acting on a cluster α is

$$\mathbf{F}_\alpha = \sum_{\beta \neq \alpha} \{ [1 - w(R_\alpha)w(R_\beta)] \mathbf{F}_{\alpha\beta}^{\text{AT}} + w(R_\alpha)w(R_\beta) \mathbf{F}_{\alpha\beta}^{\text{SCG}} \} - \mathbf{F}^{\text{TD}}(R_\alpha) \quad (1)$$

The $\mathbf{F}_{\alpha\beta}^{\text{AT}}$ and $\mathbf{F}_{\alpha\beta}^{\text{SCG}}$ are the forces between cluster α and β obtained from the AT and SCG potentials, respectively. The \mathbf{F}^{TD} is a thermodynamic (TD) force that compensates the difference in the chemical potentials of the AT and SCG resolutions^{36,68} (see section 3.1). A smooth transition from high to low resolution regimes and vice versa is enabled with the hybrid (HY) region ($R_{\text{AT}} < R < R_{\text{SCG}}$) by employing the sigmoidal function w . It is equal to 0 and 1 in the AT and SCG regions, respectively. Note that in the original implementation of AdResS, a direct interaction among AT and HY molecules is present up to one potential cutoff deep into the AT domain. Therefore, SCG interaction sites in this part of the AT domain need to be defined. This requires an additional AT region where the water molecules in the clusters are constrained to remain first neighbors as in, for example, the bundled-SPC water model. From a computational point of view, such implementation is not optimal as one would like to minimize the computationally heavy AT region. Hence, in this work, we resort to the “reverse” definition of w , as in ref 67.

Simulations are performed with the ESPResSo++ software package.⁶⁹ For the integration, we employ the standard velocity Verlet with a time step of 1 fs. We use a cubic simulation box with periodic boundary conditions and minimum image convention. The simulation box size is 9.2 nm. The temperature is maintained at 300 K with a local Langevin thermostat,⁷⁰ with the value of the friction constant equal to 5.0/ps. The geometry of the water molecules is constrained with SETTLE.⁷¹ The cutoff distance for the nonbonded interactions is $r_c = 1.2$ nm. The AT water–water nonbonded interactions are capped for very short distances (at 0.17, 0.08, and 0.14 nm, for the oxygen–oxygen, oxygen–hydrogen, and hydrogen–hydrogen interactions, respectively), that is, at distances where the corresponding radial distribution function is still zero. The reaction field method⁷² is used for the electrostatic interaction beyond the cutoff, with the dielectric

permittivity of inner and outer regions equal to 1 and 80, respectively.

Due to the long-range nature of the electrostatic interaction an efficient treatment of electrostatics, for example, Ewald summation,⁷³ in molecular simulations is imperative.^{74,75} The Ewald-type summation techniques are somewhat difficult to implement into the AdResS framework owing to the nonlocal and long-range reciprocal part of the Ewald summation.⁷⁶ Thus, as a cutoff based alternative to Ewald summation one can use, for example, the reaction field method⁷² or the screening functions,⁷⁵ which are due to the short-range interactions easier and more efficiently implemented into the domain-decomposition approaches such as AdResS. So far, in the AdResS framework, the reaction field method⁷² or the generalized reaction field method⁷⁷ have been used because they are both pairwise and short-ranged.^{2,78} However, other methods, for example, damped shifted force,^{76,79,80} can also be employed.

For the reaction field method to be accurate, it is necessary that the charges within the cutoff are isotropically distributed. In our multiscale simulations, this is not the case for the charges in the HY region due to the chargeless particles in the neighboring CG region. Hence, the reaction field method is not accurate in the HY domain. But, owing to the resolution change, the physical properties in the HY region are not accurate, in any case. Here, we would like to emphasize once again that our region of interest is the AT region, and the main objective of the AdResS approach is to reproduce the full-blown atomistic simulation properties mainly there. Contrary to the HY region, the AT region is charge-homogeneous because the HY region is in all AdResS applications at least a cutoff distance wide.⁷⁸ Our previous studies have shown that such a size of the HY region is sufficient.^{2,3,81} If some artifacts nevertheless showed up in certain situations one could always mitigate them by increasing the HY region. Thus, the reaction field treatment is justified.

The starting configuration for all simulations is an equilibrated configuration obtained after 5 ns of all-atom simulation. The equilibration runs initiated from the starting configuration are 1 ns, followed by 20 ns production runs.

3. RESULTS AND DISCUSSION

3.1. Multiscale Solvation. The AdResS scheme can couple rather loosely connected molecular representations, that is, it maintains two different models with, in general, different thermodynamic properties like pressure and chemical potential in thermodynamic equilibrium. This is accomplished with a TD force,^{35,36,68} which is calculated in an iterative manner as $\mathbf{F}_{i+1}^{\text{TD}} = \mathbf{F}_i^{\text{TD}} - C \nabla \rho_i(\mathbf{r})$. It compensates for the difference in the chemical potential at different levels of resolution and consequently removes the density undulations that are observed if the force is not applied. Typically, there is a preferential tendency of the molecules to migrate into the low resolution region and change resolution in order to lower the free energy of the system. The prefactor, $C = \frac{M}{\rho_0^2 \kappa_T}$, where ρ_0 and κ_T are the bulk density and isothermal compressibility, respectively, is in practice empirically adjusted along the process to prevent under- or overcorrection. To speed up the iteration procedure, we run simultaneously at each iteration step 6 simulations with different prefactors, and the best one is chosen for the next iteration. The used prefactors are in range [0.1–50] and decrease with increasing number of iterations. The TD force used in this work that acts on bundles' COMs in

the HY region is shown in Figure 2. To validate that the solvent density at larger distances from the protein is equal to the bulk density, we examine the normalized density profile (NDP), that is, the local density divided by the bulk density, as a function of distance from the protein's COM. The NDPs, shown in Figure 2, are computed for the water oxygen atoms and MARTINI SCG beads. The AdResS and all-atom SPC NDPs for the water oxygen atoms match well and display similar standard deviations denoted by the error bars.

3.2. SPC versus Bundled-SPC versus SPC/MARTINI Solvation. Previous papers^{58,82} have reported that the largest discrepancies between the bundled-SPC water models compared to the unrestrained SPC model are in the properties of the water itself, while as a solvent, the bundled-SPC models in most cases performed reasonably well.⁵⁰ However, taken together, small differences can have a substantial impact. For example, it was shown that both bundled-SPC solvation models can lead to the unfolding of a protein.⁸² Here, we examine the structural and dynamic properties of the solvent near the protein Trp-Cage and thus the collective solvent–solvent interactions, the properties of the protein–solvent interface, and the properties of the protein itself.

We compute the self and distinct parts of the Van Hove function $G(\mathbf{r},t)$ to obtain the structural and dynamical organization of water around the protein. In Figure 3, we

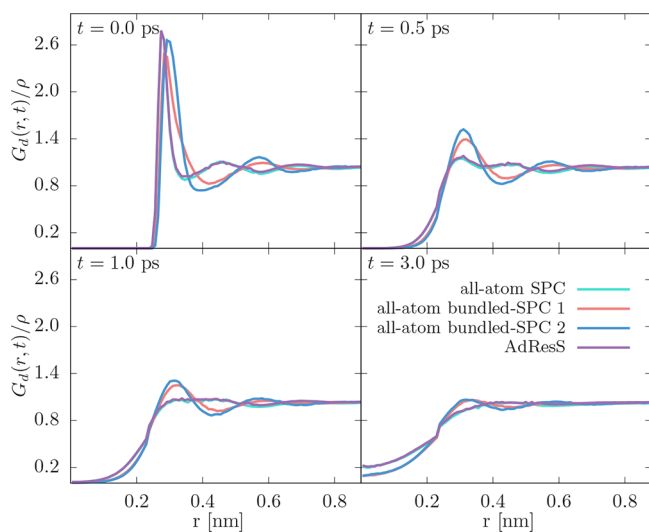


Figure 3. Distinct part of the Van Hove function $G_d(r,t)/\rho$ of water oxygen atoms within the 1–2 hydration shells at times 0, 0.5, 1.0, and 3.0 ps. We compare the results of all-atom simulations with three solvent models, that is, the SPC, bundled-SPC model 1 and 2, and the AdResS (multiscale SPC/MARTINI) solvation.

first examine the distinct part, $G_d(r,t)$, which gives the probability to find a different particle at position \mathbf{r} at time t , given that there was a particle at the origin at time $t = 0$. For isotropic fluids, $G_d(r,t) = (4\pi r^2 N)^{-1} \sum_{i \neq j} \langle \delta(r - |\mathbf{r}_i(t) - \mathbf{r}_j(0)|) \rangle$, where the double sum is performed over all pairs of N particles in the system, $\mathbf{r}_{ij}(t)$ is the position vector of the ij th atom at time t , and the brackets $\langle \dots \rangle$ denote an average over time origins. At $t = 0$, the G_d relates to the well-known radial distribution function (RDF), that is, $G_d(r,0) = \rho g(r)$. We calculated the $G_d(r,t)$ for water oxygen atoms at four different times: 0, 0.5, 1.0, and 3.0 ps. To make a relevant comparison with the fully AT simulation, we average only over water molecules that are located within a sphere, whose center

coincides with the protein's COM and has a radius of 1.6 nm. We took into account the excluded volume due to the protein and the limited region of averaging. Due to the changed Lennard-Jones parameters and the added bundled interaction in the bundled-SPC models, the RDFs are quite altered. In particular, the distributions are shifted toward larger distances especially in terms of the position of the second neighbors' peak. At later times, the G_d 's of the bundled-SPC models show more time-persistent structural correlations compared to the G_d 's of the SPC model. For AdResS simulation, the G_d 's match the reference all-atom SPC results within the line thickness thus demonstrating that not only the structural part but also the dynamical part of the water organization is fully preserved.

The self-part of the Van Hove function, $G_s(r,t) = (4\pi r^2 N)^{-1} \sum_i \langle \delta(r - |\mathbf{r}_i(t) - \mathbf{r}_i(0)|) \rangle$, probes the dynamics of a single particle in terms of its displacement from an initial position. Figure 4 shows the $G_s(r,t)$ for water oxygen atoms

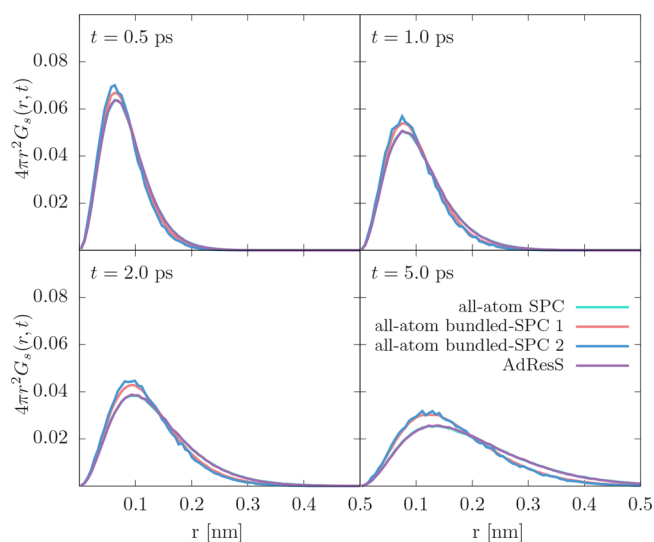


Figure 4. Self-part of the Van Hove function $4\pi r^2 G_s(r,t)$ of water oxygen atoms within the 1–2 hydration shells at times 0.5, 1.0, 2.0, and 5.0 ps.

within the 1–2 hydration shells from 0.5 to 5 ps. Multiscale solvation again gives very comparable results to the SPC, whereas the profiles for the bundled-SPC solvation are shifted toward smaller distances indicating the slowed diffusion of water molecules.

To assess the perturbation of hydrogen bond network connectivity of water due the bundles, we examine the tetrahedrality order parameter, Q_4 (Figure 5). Defined by Errington and Debenedetti⁸³ as $Q_4(x) = \langle 1 - 3/8 \sum_{i=1}^3 \sum_{j=i+1}^4 (\cos \theta_{ijk} + 1/3)^2 \rangle$, it measures the degree of local geometric tetrahedral order of the first solvation shell of a given molecule. The sum runs over distinct pairs of the four closest neighbors of the reference water molecule i , and θ_{ijk} is the angle between vectors \mathbf{r}_{ij} and \mathbf{r}_{ik} , with j and k being the nearest neighbor molecules. In the two extremes of the perfect tetrahedral geometry and an ideal disordered gas, the Q_4 takes values of 1 and 0, respectively. Near the surface of the protein, the tetrahedral order is disrupted as the water molecules form hydrogen bonds not only with neighboring water molecules but also with electronegative protein atoms. With this in mind, we calculate Q_4 by actually considering the four nearest neighbors irrespective of their identity, that is,

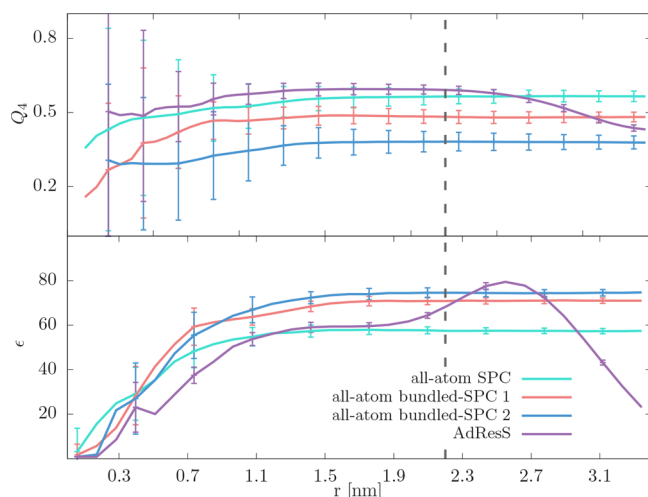


Figure 5. Tetrahedrality, Q_4 (top), and relative permittivities, ϵ (bottom), (with standard deviation denoted by the error bars) of water as a function of distance to the protein's COM. The dotted gray line indicates the boundary between the AT and HY region for multiscale simulation.

whether they pertain to water molecules or indeed to protein atoms. Compared to the SPC, the bundled-SPC has a factor of 2 lower order of tetrahedrality. In the AT region, the multiscale and SPC solvations give similar Q_4 profiles.

Differences between the SPC and bundled-SPC solvations are also found in the water's local dielectric permittivity, ϵ , which we calculate within the Kirkwood theory where it is related to the average vector sum of the dipole moments, μ , of a water molecule i centered in a spherical region S of volume V embedded into a solvent continuum ($\epsilon_{\text{RF}} = 80$),^{54,84} that is,

$$\epsilon = \frac{1 + [\rho g \mu^2 / 3 \epsilon_0 k_B T] [2 \epsilon_{\text{RF}} / (2 \epsilon_{\text{RF}} + 1)]}{1 - [\rho g \mu^2 / 3 \epsilon_0 k_B T] [1 / (2 \epsilon_{\text{RF}} + 1)]};$$

$$g = 1 + \left\langle \sum_{j \in S} \cos \theta_{ij} \right\rangle_i \quad (2)$$

The dipole density ρ is calculated as $\langle N_i / (V - V_{\text{ex},i}) \rangle_i$, where N_i is the number of water molecules with indices $j = 1, N_i$ in the Kirkwood sphere S around the reference water molecule i . $\langle \dots \rangle_i$ denotes an average over all water molecules in the set, θ_{ij} is the angle between dipoles of water molecules i and j , k_B is the Boltzmann constant, T is the temperature, and $V_{\text{ex},i}$ is the excluded volume due to protein atoms. The spatially varying profile of ϵ is then obtained with discretization of distances from the protein molecule into bins and calculating the average $\langle \dots \rangle_i$ in eq 2, over water molecules that belong to a particular bin. The profiles are shown in Figure 5. For all solvations, we observe a decrease in the local dielectric response for water proximal to protein due to immobilized water molecules in its vicinity. In the bulk, $\epsilon = 58, 71, 75$, and 60 for the SPC, bundled-SPC 1, bundled-SPC 2, and (AT region) AdResS solvations, respectively. From the plotted standard deviations, one can see that in the vicinity of the protein, ϵ varies substantially and depends on the current configuration of the protein. Moreover, there the statistics is lower due to a smaller number of water molecules. However, in the bulk water regime (distances beyond 1.1 nm), the statistics is improved and the average values of the AdResS and all-atom solvations match. In the HY region, we observe deviations due to the added bundled interaction and the switch-off of the electrostatic interactions,

which freeze the rotational degrees of freedom of water molecules and thus lower the dielectric constant. This effect was observed also in the previous studies.⁵⁴ An alternative route to the dielectric permittivity computation is via fluctuations of the total dipole moment. One could compute also the total dipole moment fluctuations from water molecules residing in spherical regions of growing radii centered at the protein's COM as in ref 85. However, here we are interested in the perturbations induced by the resolution boundary. Thus, we compute the local rather than the global dielectric permittivity from which this effect cannot be discerned.

The properties of the protein–solvent interface are investigated with the protein–water hydrogen bond network. We employ the standard geometric criterion,^{86,87} where the acceptor and donor are hydrogen bonded if the distance between the donor and acceptor is smaller than 0.35 nm and the donor–hydrogen–acceptor angle is less than 30°. We investigate the average total number, N_{hb} , and lifetime of hydrogen bonds, $\tau(C_{\text{hb}})$, formed between the protein and the surrounding water molecules. The average lifetime can be extracted from the relaxation of the correlation function $C_{\text{hb}}(t) = \langle h(0)h(t) \rangle / \langle h^2(0) \rangle$, where $h(t)$ has the value of 1 if a particular pair is hydrogen bonded at time t , and 0 otherwise. Additionally, we study the average occupancy and residence time. The occupancy, N_r , is an average number of water molecules residing in the first hydration shell of protein atoms, whereas the residence time gives the estimated rearrangement time of the solvent shells around the protein. To this end, we compute the residence autocorrelation function, $C_r(t) = \langle n(0)n(t) \rangle / \langle n^2(0) \rangle$, where $n(t) = 1$ if at time t the water molecule is located within a specified distance (0.35 nm in our case) of the protein atom and 0 otherwise. $C_r(t)$ can be integrated to yield the residence times, $\tau(C_r)$. The hydrogen bond and residential analyses are presented in Figure 6. Within error bars, AdResS simulations match the reference SPC solvation results. In comparison, the bundled-SPC solvations results show some discrepancies, that is, the average number and lifetime of hydrogen bonds is somewhat lower for the bundled-SPC solvations, while the residence times are increased.

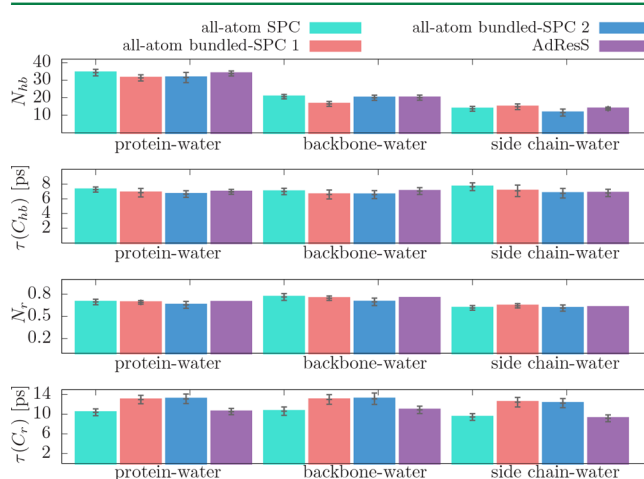


Figure 6. Average total number, N_{hb} , and lifetime, $\tau(C_{\text{hb}})$, of hydrogen bonds formed between the protein and the surrounding water molecules. Average occupancy, N_r , and residence time, $\tau(C_r)$, of water molecules in the first hydration shell of the protein atoms. The error bars denote the standard deviation.

For all investigated solvations, the protein remains in the folded conformation throughout the simulation. To show this point, we plot, in Figure 7, the radius of gyration, R_g , root-

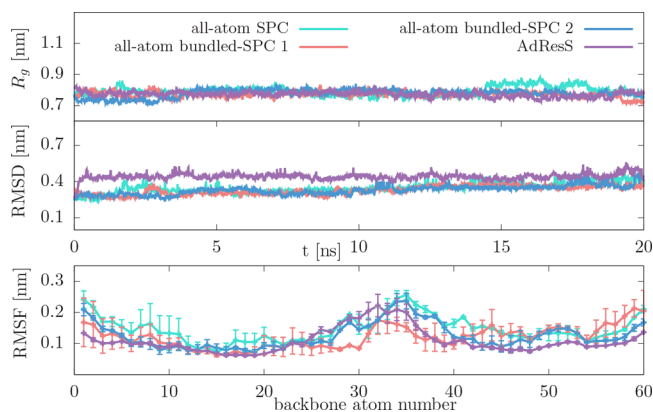


Figure 7. (top) Radius of gyration (R_g) as a function of the simulation time. (middle and bottom) Root-mean-square deviation (RMSD) and fluctuations (RMSF) of the backbone atoms with respect to the crystal structure. The configuration snapshots were prior to RMSD calculation superimposed on the initial crystal structure (1L2Y.pdb). The error bars of RMSF denote the standard deviation computed by block averaging.

mean-square deviation (RMSD), and root-mean-square fluctuations (RMSF) of the protein's backbone atoms with respect to the crystal initial structure. We have chosen to test the Trp-Cage miniprotein in our simulations because of the fast dynamics of this protein,^{88–90} that is, at room temperature the experimentally observed folding time is only 4 μ s.⁹¹ Moreover, the temperature induced denaturation is even faster. For example, it was reported that in MD simulations the Trp-Cage protein unfolds in the first few nanoseconds at 400 K.⁹² Thus, other nontemperature perturbations, such as the multiscale or bundled-SPC solvations, should be observed on the time scales of our simulations. Here, we do not observe such an effect. For the all-atom SPC and the multiscale solvations, unfolding is not expected as the experimental denaturation temperature of the Trp-Cage is about 315 K.⁹² For the bundled-SPC solvations, which were shown to lead to the partial unfolding of the coiled-coil dimer,⁸² the reason for unfolding not to be observed may be because the modified water model does not affect the stability of the Trp-Cage, due to the simulation length, or more likely due to the overstabilizing protein force field. Namely, in MD simulations, the observed melting temperatures are significantly higher than experimental ones ranging from 360 to 450 K depending on the force field used.⁹² Nonetheless, the primary goal of our work is not to uncover the (un)folding process of the Trp-Cage protein but rather to demonstrate that there are no unphysical artifacts due to the multiscale simulations. The study of folding process is feasible also with multiscale simulations; however, in that case, one should use the flexible boundary domains to adjust to the geometry of the unfolded protein.^{52,93}

4. CONCLUSIONS

Solvent plays a vital role in biological processes, with hydration water critically impacting the structure, stability, dynamics, and function of biomolecules. The proper description of solution is thus required in simulations of bioentities such as proteins. In this work, we have demonstrated how the accuracy of the high

resolution all-atom solution can still be maintained with the computationally efficient multiscale simulations even when the coupling is supramolecular. In particular, we achieved this by applying AdResS in conjunction with the SWINGER algorithm that assembles, disassembles, and reassembles clusters as needed during the course of the simulation. Owing to SWINGER, the standard AT water models can be used in the region of interest, which are seamlessly coupled to the supramolecular models. We found good agreement of the multiscale results with the corresponding simulations using the SPC model. This includes the structural and dynamic properties of solution (i.e., spatiotemporal Van Hove functions, tetrahedrality, and dielectric permittivity), the protein–solvent interaction properties (i.e., the characteristics of hydrogen-bonding, occupancy, and residence time), and the structural properties of the protein (i.e., the root-mean-square deviation, fluctuations, and the radius of gyration). Our approach is general and can be applied to any standard atomistic force field to be coupled with the MARTINI or any other supramolecular CG force field.

■ AUTHOR INFORMATION

Corresponding Author

*E-mail: praprot@cmm.ki.si.

ORCID

Matej Praprotnik: 0000-0003-0825-1659

Notes

The authors declare no competing financial interest.

■ ACKNOWLEDGMENTS

J.Z. acknowledges financial support as an ETH Zurich Fellow. M.P. acknowledges financial support from the Slovenian Research Agency (research core funding No. P1-0002 and the project J1-7435).

■ REFERENCES

- (1) Ayton, G. S.; Noid, W. G.; Voth, G. A. Multiscale modeling of biomolecular systems: In serial and in parallel. *Curr. Opin. Struct. Biol.* **2007**, *17*, 192–198.
- (2) Praprotnik, M.; Delle Site, L.; Kremer, K. Multiscale simulation of soft matter: From scale bridging to adaptive resolution. *Annu. Rev. Phys. Chem.* **2008**, *59*, 545–571.
- (3) Delle Site, L.; Praprotnik, M. Molecular systems with open boundaries: Theory and Simulation. *Phys. Rep.* **2017**, *693*, 1–56.
- (4) Han, W.; Wan, C. K.; Jiang, F.; Wu, Y. D. PACE Force Field for Protein Simulations. 1. Full Parameterization of Version 1 and Verification. *J. Chem. Theory Comput.* **2010**, *6*, 3373–3389.
- (5) Han, W.; Schulten, K. Further optimization of a hybrid united-atom and coarse-grained force field for folding simulations: Improved backbone hydration and interactions between charged side chains. *J. Chem. Theory Comput.* **2012**, *8*, 4413–4424.
- (6) Michel, J.; Orsi, M.; Essex, J. W. Prediction of partition coefficients by multiscale hybrid atomic-level/coarse-grain simulations. *J. Phys. Chem. B* **2008**, *112*, 657–660.
- (7) Orsi, M.; Ding, W.; Palaiokostas, M. Direct mixing of atomistic solutes and coarse-grained water. *J. Chem. Theory Comput.* **2014**, *10*, 4684–4693.
- (8) Gonzalez, H. C.; Darré, L.; Pantano, S. Transferable mixing of atomistic and coarse-grain water models. *J. Phys. Chem. B* **2013**, *117*, 14438–14448.
- (9) Kar, P.; Feig, M. Hybrid All-Atom/Coarse-Grained Simulations of Proteins by Direct Coupling of CHARMM and PRIMO Force Fields. *J. Chem. Theory Comput.* **2017**, *13*, 5753.
- (10) Riniker, S.; Eichenberger, A. P.; van Gunsteren, W. F. Solvating atomic level fine-grained proteins in supra-molecular level coarse-

grained water for molecular dynamics simulations. *Eur. Biophys. J.* **2012**, *41*, 647–661.

(11) Masella, M.; Borgis, D.; Cuniasse, P. Combining a polarizable force-field and a coarse-grained polarizable solvent model: Application to long dynamics simulations of bovine pancreatic trypsin inhibitor. *J. Comput. Chem.* **2008**, *29*, 1707–1724.

(12) Masella, M.; Borgis, D.; Cuniasse, P. Combining a polarizable force-field and a coarse-grained polarizable solvent model. II. Accounting for hydrophobic effects. *J. Comput. Chem.* **2011**, *32*, 2664–2678.

(13) Shelley, M. Y.; Selvan, M. E.; Zhao, J.; Babin, V.; Liao, C.; Li, J.; Shelley, J. C. A New Mixed All-Atom/Coarse-Grained Model: Application to Melittin Aggregation in Aqueous Solution. *J. Chem. Theory Comput.* **2017**, *13*, 3881–3897.

(14) Shi, Q.; Izvekov, S.; Voth, G. A. Mixed atomistic and coarse-grained molecular dynamics: Simulation of a membrane-bound ion channel. *J. Phys. Chem. B* **2006**, *110*, 15045–15048.

(15) Lu, L.; Dama, J. F.; Voth, G. A. Fitting coarse-grained distribution functions through an iterative force-matching method. *J. Chem. Phys.* **2013**, *139*, 121906.

(16) Rzepiela, A. J.; Louhivuori, M.; Peter, C.; Marrink, S. J. Hybrid simulations: Combining atomistic and coarse-grained force fields using virtual sites. *Phys. Chem. Chem. Phys.* **2011**, *13*, 10437–10448.

(17) Wassenaar, T. A.; Ingólfsson, H. L.; Priess, M.; Marrink, S. J.; Schaefer, L. V. Mixing MARTINI: Electrostatic coupling in hybrid atomistic - coarse-grained biomolecular simulations. *J. Phys. Chem. B* **2013**, *117*, 3516–3530.

(18) Sokkar, P.; Choi, S. M.; Rhee, Y. M. Simple method for simulating the mixture of atomistic and coarse-grained molecular systems. *J. Chem. Theory Comput.* **2013**, *9*, 3728–3739.

(19) Luchko, T.; Gusarov, S.; Roe, D. R.; Simmerling, C.; Case, D. A.; Tuszynski, J.; Kovalenko, A. Three-Dimensional Molecular Theory of Solvation Coupled with Molecular Dynamics in Amber. *J. Chem. Theory Comput.* **2010**, *6*, 607–624.

(20) Brancato, G.; et al. A mean field approach for molecular simulations of fluid systems. *J. Chem. Phys.* **2005**, *122*, 154109.

(21) Brancato, G.; Rega, N.; Barone, V. Reliable molecular simulations of solute-solvent systems with a minimum number of solvent shells. *J. Chem. Phys.* **2006**, *124*, 214505.

(22) King, G.; Warshel, A. A surface constrained allatom solvent model for effective simulations of polar solutions. *J. Chem. Phys.* **1989**, *91*, 3647.

(23) Okur, A.; Simmerling, C. In *Hybrid Explicit/Implicit Solvation Methods*; Spellmeyer, D. C., Ed.; Annual Reports in Computational Chemistry; Elsevier, 2006; Vol. 2; pp 97–109.

(24) Roux, B.; Simonson, T. Implicit solvent models. *Biophys. Chem.* **1999**, *78*, 1–20.

(25) Mondal, S.; Mukherjee, S.; Bagchi, B. Origin of diverse time scales in the protein hydration layer solvation dynamics: A simulation study. *J. Chem. Phys.* **2017**, *147*, 154901.

(26) Sokkar, P.; Boulanger, E.; Thiel, W.; Sanchez-Garcia, E. Hybrid quantum mechanics/molecular mechanics/coarse grained modeling: A triple-resolution approach for biomolecular systems. *J. Chem. Theory Comput.* **2015**, *11*, 1809–1818.

(27) Riniker, S.; Eichenberger, A. P.; van Gunsteren, W. F. Structural effects of an atomic-level layer of water molecules around proteins solvated in supra-molecular coarse-grained water. *J. Phys. Chem. B* **2012**, *116*, 8873–8879.

(28) Kuhn, A. B.; Gopal, S. M.; Schäfer, L. V. On using atomistic solvent layers in hybrid all-atom/coarse-grained molecular dynamics simulations. *J. Chem. Theory Comput.* **2015**, *11*, 4460–4472.

(29) Nielsen, S. O.; Moore, P. B.; Ensing, B. Adaptive multiscale molecular dynamics of macromolecular fluids. *Phys. Rev. Lett.* **2010**, *105*, 237802.

(30) Shen, L.; Hu, H. Resolution-adapted all-atomic and coarse-grained model for biomolecular simulations. *J. Chem. Theory Comput.* **2014**, *10*, 2528–2536.

(31) Alekseeva, U.; Winkler, R. G.; Sutmann, G. Hydrodynamics in adaptive resolution particle simulations: Multiparticle collision dynamics. *J. Comput. Phys.* **2016**, *314*, 14–34.

(32) Petsev, N. D.; Leal, L. G.; Shell, M. S. Hybrid molecular-continuum simulations using smoothed dissipative particle dynamics. *J. Chem. Phys.* **2015**, *142*, 044101.

(33) Petsev, N. D.; Leal, L. G.; Shell, M. S. Coupling discrete and continuum concentration particle models for multiscale and hybrid molecular-continuum simulations. *J. Chem. Phys.* **2017**, *147*, 234112.

(34) Praprotnik, M.; Delle Site, L.; Kremer, K. Adaptive resolution molecular-dynamics simulation: Changing the degrees of freedom on the fly. *J. Chem. Phys.* **2005**, *123*, 224106.

(35) Poblete, S.; Praprotnik, M.; Kremer, K.; Delle Site, L. Coupling different levels of resolution in molecular simulations. *J. Chem. Phys.* **2010**, *132*, 114101.

(36) Fritsch, S.; Poblete, S.; Junghans, C.; Ciccotti, G.; Delle Site, L.; Kremer, K. Adaptive resolution molecular dynamics simulation through coupling to an internal particle reservoir. *Phys. Rev. Lett.* **2012**, *108*, 170602.

(37) Wang, H.; Hartmann, C.; Schütte, C.; Delle Site, L. Grand-canonical-like molecular-dynamics simulations by using an adaptive-resolution technique. *Phys. Rev. X* **2013**, *3*, 011018.

(38) Agarwal, A.; Delle Site, L. Path integral molecular dynamics within the grand canonical-like adaptive resolution technique: Simulation of liquid water. *J. Chem. Phys.* **2015**, *143*, 094102.

(39) Delle Site, L. Formulation of Liouville's theorem for grand ensemble molecular simulations. *Phys. Rev. E: Stat. Phys., Plasmas, Fluids, Relat. Interdiscip. Top.* **2016**, *93*, 022130.

(40) Delle Site, L. Grand Canonical Adaptive Resolution Simulation for Molecules with Electrons: A Theoretical Framework based on Physical Consistency. *Comput. Phys. Commun.* **2018**, *222*, 94.

(41) Potestio, R.; Fritsch, S.; Español, P.; Delgado-Buscalioni, R.; Kremer, K.; Everaers, R.; Donadio, D. Hamiltonian adaptive resolution simulation for molecular liquids. *Phys. Rev. Lett.* **2013**, *110*, 108301.

(42) Potestio, R.; Español, P.; Delgado-Buscalioni, R.; Everaers, R.; Kremer, K.; Donadio, D. Monte Carlo adaptive resolution simulation of multicomponent molecular liquids. *Phys. Rev. Lett.* **2013**, *111*, 060601.

(43) Español, P.; Delgado-Buscalioni, R.; Everaers, R.; Potestio, R.; Donadio, D.; Kremer, K. Statistical mechanics of hamiltonian adaptive resolution simulations. *J. Chem. Phys.* **2015**, *142*, 064115.

(44) Delgado-Buscalioni, R.; Sablić, J.; Praprotnik, M. Open boundary molecular dynamics. *Eur. Phys. J.: Spec. Top.* **2015**, *224*, 2331–2349.

(45) Sablić, J.; Praprotnik, M.; Delgado-Buscalioni, R. Open boundary molecular dynamics of sheared star-polymer melts. *Soft Matter* **2016**, *12*, 2416–2439.

(46) Sablić, J.; Praprotnik, M.; Delgado-Buscalioni, R. Deciphering the dynamics of star molecules in shear flow. *Soft Matter* **2017**, *13*, 4971–4987.

(47) Sablić, J.; Delgado-Buscalioni, R.; Praprotnik, M. Application of the Eckart frame to soft matter: rotation of star polymers under shear flow. *Soft Matter* **2017**, *13*, 6988–7000.

(48) Christen, M.; van Gunsteren, W. F. Multigraining: An algorithm for simultaneous fine-grained and coarse-grained simulation of molecular systems. *J. Chem. Phys.* **2006**, *124*, 154106.

(49) Krajniak, J.; Pandiyan, S.; Nies, E.; Samaey, G. A generic adaptive resolution method for reverse mapping of polymers from coarse-grained to atomistic descriptions. *J. Chem. Theory Comput.* **2016**, *12*, 5549–5562.

(50) Zavadlav, J.; Melo, M. N.; Marrink, S. J.; Praprotnik, M. Adaptive resolution simulation of an atomistic protein in MARTINI water. *J. Chem. Phys.* **2014**, *140*, 054114.

(51) Fogarty, A. C.; Potestio, R.; Kremer, K. A multi-resolution model to capture both global fluctuations of an enzyme and molecular recognition in the ligand-binding site. *Proteins: Struct., Funct., Genet.* **2016**, *84*, 1902–1913.

- (52) Kreis, K.; Potestio, R.; Kremer, K.; Fogarty, A. C. Adaptive resolution simulations with self-adjusting high-resolution regions. *J. Chem. Theory Comput.* **2016**, *12*, 4067–4081.
- (53) Tarenzi, T.; Calandrini, V.; Potestio, R.; Giorgetti, A.; Carloni, P. Open Boundary Simulations of Proteins and Their Hydration Shells by Hamiltonian Adaptive Resolution Scheme. *J. Chem. Theory Comput.* **2017**, *13*, 5647.
- (54) Zavadlav, J.; Podgornik, R.; Praprotnik, M. Adaptive resolution simulation of a DNA molecule in salt solution. *J. Chem. Theory Comput.* **2015**, *11*, 5035–5044.
- (55) Zavadlav, J.; Podgornik, R.; Melo, M. N.; Marrink, S. J.; Praprotnik, M. Adaptive resolution simulation of an atomistic DNA molecule in MARTINI salt solution. *Eur. Phys. J.: Spec. Top.* **2016**, *225*, 1595–1607.
- (56) Zavadlav, J.; Podgornik, R.; Praprotnik, M. Order and interactions in DNA arrays: Multiscale molecular dynamics simulation. *Sci. Rep.* **2017**, *7*, 4775.
- (57) Netz, P. A.; Potestio, R.; Kremer, K. Adaptive resolution simulation of oligonucleotides. *J. Chem. Phys.* **2016**, *145*, 234101.
- (58) Fuhrmans, M.; Sanders, B. P.; Marrink, S. J.; de Vries, A. H. Effects of bundling on the properties of the SPC water model. *Theor. Chem. Acc.* **2010**, *125*, 335–344.
- (59) Zavadlav, J.; Melo, M. N.; Cunha, A. V.; de Vries, A. H.; Marrink, S. J.; Praprotnik, M. Adaptive resolution simulation of MARTINI solvents. *J. Chem. Theory Comput.* **2014**, *10*, 2591–2598.
- (60) Zavadlav, J.; Melo, M. N.; Marrink, S. J.; Praprotnik, M. Adaptive resolution simulation of polarizable supramolecular coarse-grained water models. *J. Chem. Phys.* **2015**, *142*, 244118.
- (61) Nagarajan, A.; Junghans, C.; Matysiak, S. Multiscale simulation of liquid water using a four-to-one mapping for coarse-graining. *J. Chem. Theory Comput.* **2013**, *9*, 5168–5175.
- (62) Zavadlav, J.; Marrink, S. J.; Praprotnik, M. Adaptive resolution simulation of supramolecular water: The concurrent making, breaking, and remaking of water bundles. *J. Chem. Theory Comput.* **2016**, *12*, 4138–4145.
- (63) Berendsen, H. J. C.; Postma, J. P. M.; van Gunsteren, W. F.; Hermans, J. Interaction models for water in relation to protein hydration. *Intermolecular Forces* **1981**, *14*, 331–342.
- (64) Marrink, S. J.; Risselada, H. J.; Yefimov, S.; Tieleman, D. P.; de Vries, A. H. The MARTINI force field: Coarse grained model for biomolecular simulations. *J. Phys. Chem. B* **2007**, *111*, 7812–7824.
- (65) Schmid, N.; Eichenberger, A. P.; Choutko, A.; Riniker, S.; Winger, M.; Mark, A. E.; van Gunsteren, W. F. Definition and testing of the GROMOS force-field versions 54A7 and 54B7. *Eur. Biophys. J.* **2011**, *40*, 843–856.
- (66) Marrink, S. J.; de Vries, A. H.; Mark, A. E. Coarse grained model for semiquantitative lipid simulations. *J. Phys. Chem. B* **2004**, *108*, 750–760.
- (67) Zavadlav, J.; Praprotnik, M. Adaptive resolution simulations coupling atomistic water to dissipative particle dynamics. *J. Chem. Phys.* **2017**, *147*, 114110.
- (68) Praprotnik, M.; Poblete, S.; Kremer, K. Statistical physics problems in adaptive resolution computer simulations of complex fluids. *J. Stat. Phys.* **2011**, *145*, 946–966.
- (69) Halverson, J. D.; Brandes, T.; Lenz, O.; Arnold, A.; Bevc, S.; Starchenko, V.; Kremer, K.; Stuehn, T.; Reith, D. ESPResSo++: A modern multiscale simulation package for soft matter systems. *Comput. Phys. Commun.* **2013**, *184*, 1129–1149.
- (70) Grest, G. S.; Kremer, K. Molecular-dynamics simulation for polymers in the presence of a heat bath. *Phys. Rev. A: At., Mol., Opt. Phys.* **1986**, *33*, 3628–3631.
- (71) Miyamoto, S.; Kollman, P. A. SETTLE: An analytical version of the SHAKE and RATTLE algorithm for rigid water models. *J. Comput. Chem.* **1992**, *13*, 952–962.
- (72) Neumann, M. The dielectric constant of water. Computer simulations with the MCY potential. *J. Chem. Phys.* **1985**, *82*, 5663–5672.
- (73) Ewald, P. P. Die Berechnung optischer und elektrostatischer Gitterpotentiale. *Ann. Phys.* **1921**, *369*, 253–287.
- (74) Cisneros, G. A.; Karttunen, M.; Ren, P.; Sagui, C. Classical electrostatics for biomolecular simulations. *Chem. Rev.* **2014**, *114*, 779–814.
- (75) Vatamanu, J.; Borodin, O.; Bedrov, D. Application of Screening Functions as Cut-off Based Alternative to Ewald Summation in Molecular Dynamics Simulations Using Polarizable Force Fields. *J. Chem. Theory Comput.* **2018**, *14*, 768.
- (76) Heidari, M.; Cortes-Huerto, R.; Donadio, D.; Potestio, R. Accurate and general treatment of electrostatic interaction in Hamiltonian adaptive resolution simulations. *Eur. Phys. J.: Spec. Top.* **2016**, *225*, 1505–1526.
- (77) Tironi, I. G.; Sperb, R.; Smith, P. E.; van Gunsteren, W. F. A generalized reaction field method for molecular dynamics simulations. *J. Chem. Phys.* **1995**, *102*, 5451–5459.
- (78) Praprotnik, M.; Matysiak, S.; Delle Site, L.; Kremer, K.; Clementi, C. Adaptive resolution simulation of liquid water. *J. Phys.: Condens. Matter* **2007**, *19*, 292201.
- (79) Wolf, D.; Keblinski, P.; Philippot, S. R.; Eggebrecht, J. Exact method for the simulation of Coulombic systems by spherically truncated, pairwise r^{-1} summation. *J. Chem. Phys.* **1999**, *110*, 8254.
- (80) Fennell, C. J.; Gezelter, J. D. Is the Ewald summation still necessary? Pairwise alternatives to the accepted standard for long-range electrostatics. *J. Chem. Phys.* **2006**, *124*, 234104.
- (81) Zavadlav, J.; Bevc, S.; Praprotnik, M. Adaptive resolution simulations of biomolecular systems. *Eur. Biophys. J.* **2017**, *46*, 821.
- (82) Gopal, S. M.; Kuhn, A. B.; Schäfer, L. V. Systematic evaluation of bundled SPC water for biomolecular simulations. *Phys. Chem. Chem. Phys.* **2015**, *17*, 8393–8406.
- (83) Errington, J. R.; Debenedetti, P. G. Relationship between structural order and the anomalies of liquid water. *Nature* **2001**, *409*, 318–321.
- (84) Young, M. A.; Jayaram, B.; Beveridge, D. L. Local dielectric environment of B-DNA in solution: Results from a 14 ns molecular dynamics trajectory. *J. Phys. Chem. B* **1998**, *102*, 7666–7669.
- (85) Chandramouli, B.; Zazza, C.; Mancini, G.; Brancato, G. Boundary Condition Effects on the Dynamic and Electric Properties of Hydration Layers. *J. Phys. Chem. A* **2015**, *119*, 5465–5475.
- (86) Luzar, A.; Chandler, D. Hydrogen-bond kinetics in liquid water. *Nature* **1996**, *379*, 55–57.
- (87) Luzar, A.; Chandler, D. Effect of environment on hydrogen bond dynamics in liquid water. *Phys. Rev. Lett.* **1996**, *76*, 928–931.
- (88) Meuzelaar, H.; Marino, K. A.; Huerta-Viga, A.; Panman, M. R.; Smeenk, L. E. J.; Kettelarij, A. J.; van Maarseveen, J. H.; Timmerman, P.; Bolhuis, P. G.; Woutersen, S. Folding Dynamics of the Trp-Cage Mini-protein: Evidence for a Native-Like Intermediate from Combined Time-Resolved Vibrational Spectroscopy and Molecular Dynamics Simulations. *J. Phys. Chem. B* **2013**, *117*, 11490–11501.
- (89) Kannan, S.; Zacharias, M. Role of Tryptophan Side Chain Dynamics on the Trp-Cage Mini-Protein Folding Studied by Molecular Dynamics Simulations. *PLoS One* **2014**, *9*, e88383.
- (90) Day, R.; Paschek, D.; Garcia, A. E. Microsecond simulations of the folding/unfolding thermodynamics of the Trp-cage mini-protein. *Proteins: Struct., Funct., Genet.* **2010**, *78*, 1889–1899.
- (91) Qiu, L.; Pabit, S. A.; Roitberg, A. E.; Hagen, S. J. Smaller and Faster: The 20-Residue Trp-Cage Protein Folds in 4 μ s. *J. Am. Chem. Soc.* **2002**, *124*, 12952–12953.
- (92) Gattin, Z.; Riniker, S.; Hore, P. J.; Mok, K. H.; van Gunsteren, W. F. Temperature and urea induced denaturation of the TRP-cage mini protein TCSb: A simulation study consistent with experimental observations. *Protein Sci.* **2009**, *18*, 2090–2099.
- (93) Szklarczyk, O. M.; Bieler, N. S.; Hünenberger, P. H.; van Gunsteren, W. F. Flexible Boundaries for Multiresolution Solvation: An Algorithm for Spatial Multiscaling in Molecular Dynamics Simulations. *J. Chem. Theory Comput.* **2015**, *11*, 5447–5463.